

A quantum-enhanced magnetometer using a single high-spin nucleus in silicon

Tao Xin(辛涛), Ke Zhang(张科), and Jun Li(李俊)

Citation: Chin. Phys. B, 2024, 33 (**9**): 090302. DOI: 10.1088/1674-1056/ad5a75
Journal homepage: http://cpb.iphy.ac.cn; http://iopscience.iop.org/cpb

What follows is a list of articles you may be interested in

A family of quantum von Neumann architecture

Dong-Sheng Wang(王东升)
Chin. Phys. B, 2024, 33 (**8**): 080302. DOI: 10.1088/1674-1056/ad50be

Simulations of superconducting quantum gates by digital flux tuner for qubits

Xiao Geng(耿霄), Kaiyong He(何楷泳), Jianshe Liu(刘建设), and Wei Chen(陈炜)
Chin. Phys. B, 2024, 33 (**7**): 070305. DOI: 10.1088/1674-1056/ad47ab

Electric field dependence of spin qubit in a Si-MOS quantum dot

Rong-Long Ma(马荣龙), Ming Ni(倪铭), Yu-Chen Zhou(周雨晨), Zhen-Zhen Kong(孔真真), Gui-Lei Wang(王桂磊), Di Liu(刘頔), Gang Luo(罗刚), Gang Cao(曹刚), Hai-Ou Li(李海欧), and Guo-Ping Guo(郭国平)
Chin. Phys. B, 2024, 33 (**6**): 060312. DOI: 10.1088/1674-1056/ad3812

Design of a novel hybrid quantum deep neural network in INEQR images classification

Shuang Wang(王爽), Ke-Han Wang(王柯涵), Tao Cheng(程涛), Run-Sheng Zhao(赵润盛), Hong-Yang Ma(马鸿洋), and Shuai Guo(郭帅)
Chin. Phys. B, 2024, 33 (**6**): 060310. DOI: 10.1088/1674-1056/ad342e

Enhanced measurement precision with continuous interrogation during dynamical decoupling

Jun Zhang(张军), Peng Du(杜鹏), Lei Jing(敬雷), Peng Xu(徐鹏), Li You(尤力), and Wenxian Zhang(张文献)
Chin. Phys. B, 2024, 33 (**3**): 030301. DOI: 10.1088/1674-1056/ad1985

SPECIAL TOPIC — Quantum computing and quantum sensing

A quantum-enhanced magnetometer using a single high-spin nucleus in silicon

Tao Xin(辛涛)[1,2,†], Ke Zhang(张科)[3,‡], and Jun Li(李俊)[4,5,1,§]

[1] *Shenzhen Institute for Quantum Science and Engineering, Southern University of Science and Technology, Shenzhen* 518055, *China*
[2] *Guangdong Provincial Key Laboratory of Quantum Science and Engineering, Southern University of Science and Technology, Shenzhen* 518055, *China*
[3] *Physikalisch-Technische Bundesanstalt, Bundesallee* 100, 38116 *Braunschweig, Germany*
[4] *Institute of Quantum Precision Measurement, State Key Laboratory of Radio Frequency Heterogeneous Integration, Shenzhen University, Shenzhen* 518060, *China*
[5] *College of Physics and Optoelectronic Engineering, Shenzhen University, Shenzhen* 518060, *China*

(Received 7 April 2024; revised manuscript received 17 June 2024; accepted manuscript online 21 June 2024)

Quantum enhanced metrology has the potential to go beyond the standard quantum limit and eventually to the ultimate Heisenberg bound. In particular, quantum probes prepared in nonclassical coherent states have recently been recognized as a useful resource for metrology. Hence, there has been considerable interest in constructing magnetic quantum sensors that combine high resolution and high sensitivity. Here, we explore a nanoscale magnetometer with quantum-enhanced sensitivity, based on ^{123}Sb ($I = 7/2$) nuclear spin doped in silicon, that takes advantage of techniques of spin-squeezing and coherent control. With the optimal squeezed initial state, the magnetic field sensitivity may be expected to approach 6 aT·Hz$^{-1/2}$·cm$^{-3/2}$ and 603 nT·Hz$^{-1/2}$ at the single-spin level. This magnetic sensor may provide a novel sensitive and high-resolution route to microscopic mapping of magnetic fields as well as other applications.

Keywords: quantum magnetometer, silicon quantum qubit, nuclear electrical resonance

PACS: 03.67.Lx, 03.67.–a, 42.50.Dv **DOI:** 10.1088/1674-1056/ad5a75

1. Introduction

Quantum sensors capable of detecting very weak magnetic fields have attracted tremendous interest in recent years.[1] They hold great promise, especially in the areas of testing fundamental physics,[2,3] probing condensed matter systems,[4] magnetoencephalography[5] and magnetic resonance imaging,[6] to name a few. A significant challenge in this field is to construct magnetometers with both high sensitivity and high spatial resolution, which are critical for a variety of applications such as local mapping of fields in nanodevices, probing magnetic single molecules,[7] and close-up biological imaging. For instance, superconducting quantum interference devices[8] and atomic magnetometers[9,10] are at the forefront of magnetic sensitivities, but their detection volumes are limited by the bulky size of the order of cm^3. On the other hand, certain platforms including those with atoms,[11] ions,[12] or quantum defects in solids[13] may achieve spatial resolution on scales from micrometers to nanometers, but this advantage is offset by a relatively low sensitivity. One prominent example is the nitrogen-vacancy (NV) center in diamond, which features excellent quantum coherence properties and atomic-scale size,[14–19] yet still needs substantial improvement to reach the theoretical sensitivity limit.[19] Therefore, enhancing the sensitivity of nanoscale magnetometers continues to be a topic of active research.

The paradigm for nanoscale sensing is a single quantum system, such as a single atom[20,21] or the electron spin of a single NV center,[14,15] being coupled to an environment under investigation. Two energy levels of the system are chosen to probe the environmental magnetic field, following the Ramsey measurement protocol. The achievable precision is known to be bounded by the standard quantum limit (SQL). To obtain better accuracy without sacrificing much spatial resolution, it is natural to go beyond two-level magnetometry. That is, we can involve more energy levels in the sensing process so that quantum properties will play a non-trivial role. First, this allows the creation of higher-order quantum coherences, which increase the accumulated phase during the interrogation time. For instance, it has been demonstrated for NV centers in diamond that double-quantum magnetometry using all three magnetic sublevels of electrons can be twice as sensitive as single-quantum magnetometry.[22] Then, nonclassical states can be harnessed to extend sensing capabilities. Over the years, magnetometry utilizing quantum effects like squeezing or entanglement has been extensively studied on various platforms.[10,23] Overall, quantum-enhanced sensing can generally achieve increase of precision by a factor intermediate

†Corresponding author. E-mail: xint@sustech.edu.cn
‡Corresponding author. E-mail: kezhang@uni-mainz.de
§Corresponding author. E-mail: lijunquantum@szu.edu.cn

© 2024 Chinese Physical Society and IOP Publishing Ltd

between the SQL and the Heisenberg limit.

Recent successes in coherent electrical control and single shot readout of single high-spin nuclei in quantum dots have opened new possibilities for physical realizations of multilevel magnetometry.[24,25] In this work, we study this candidate magnetometer system with a focus on sensitivity. Several previous works have demonstrated how quadrupole interactions can be used to generate quantum squeezing for ensembles of nuclear spins.[26,27] In the following, we analogously exploit the physical properties of quadrupolar nuclei to generate nonclassical states such that the uncertainty is reduced along the detection direction to achieve quantum enhanced sensitivity. The crucial difference here is that we are using a single nucleus and thus have the advantage of high spatial resolution.

2. Scheme

The magnetometer is provided by an ionized atom (^{123}Sb) implanted in a metal–oxide–semiconductor nanostructure with isotopically enriched ^{28}Si fabricated on it; see Fig. 1(a). The ^{123}Sb donor is confined in a nanoscale region (about 10 nm in size) and hence can be brought in direct proximity to a magnetic-field source, such as an electron or nuclear spin. ^{123}Sb has a nuclear spin quantum number $I = 7/2$ so that the dimension of the Hilbert space $2I+1 = 8$. Under a large quantization magnetic field $\boldsymbol{B}_0 = B_0\hat{z}$, the nuclear spin eigenstates can be seen as separable from those of the electron spin. Then, via an electron spin assisted pumping technique developed in Ref. [24], the ^{123}Sb nucleus can be spin-polarized in any state $|m\rangle$ ($m = -7/2, \ldots, 7/2$). The structure contains some electrostatic gates to control the electrochemical potential of the donor. For measurement, a single-electron transistor (SET) based on energy-selective electron tunneling into a cold charge reservoir is employed for single-shot electron spin readout.

The canonical approach for detecting magnetic field employs the Ramsey-type sequence as shown in Fig. 1(b). The system starts from the state $|\psi_i\rangle = |+7/2\rangle$, and then is rotated by an angle $\pi/2$ about the y-axis in the equatorial plane, giving a state pointing in the x-axis direction. The state then undergoes an evolution of duration t governed by the Hamiltonian $\hat{H} = \omega\hat{I}_z$ induced by the magnetic field B to be detected, here $\omega = \gamma B$, with γ being the gyromagnetic ratio of the nucleus. During this evolution, a phase $\phi = \omega t$ parameter is encoded into the system dynamics. Finally, in the measurement stage, the information of the encoded phase ϕ is extracted from measuring the spin component I_x of the final state. It is a well-known result that this basic Ramsey measurement scheme for estimating ϕ leads to a minimum phase uncertainty $\Delta\phi_{\mathrm{SQL}} = 1/\sqrt{2I}$, corresponding to the standard quantum limit.[28]

Now let us look at the general metrology scheme,[29] as shown in Fig. 1(c). Before magnetic field sensing, we apply a unitary transform to get a general probe state $|\psi_{\mathrm{p}}\rangle$. There is a certain direction $\hat{\boldsymbol{n}}$ to which the evolution of $|\psi_{\mathrm{p}}\rangle$ is most magnetic-sensitive. We can simply add a frame transformation that turns $\hat{\boldsymbol{n}}$ into the magnetic field direction that we intend to measure. Suppose at the measurement time t we arrive at the state $|\psi_t\rangle = \mathrm{e}^{-\mathrm{i}\phi\hat{I}_z}|\psi_{\mathrm{p}}\rangle$, and we make measurements on the observable $\hat{\mathcal{O}}$. The expectation value will be

$$\langle\hat{\mathcal{O}}\rangle = \langle\psi_{\mathrm{p}}|\mathrm{e}^{-\mathrm{i}\phi\hat{I}_z}\hat{\mathcal{O}}\,\mathrm{e}^{\mathrm{i}\phi\hat{I}_z}|\psi_{\mathrm{p}}\rangle. \tag{1}$$

According to the parameter estimation theory, the unavoidable fluctuation of the outcomes of $\hat{\mathcal{O}}$ induces uncertainty on the estimation of ϕ, which can be characterized by the error propagation formula $\Delta\phi = \Delta\hat{\mathcal{O}}\cdot\left|\partial_\phi\langle\hat{\mathcal{O}}\rangle\right|^{-1}$, where $\left|\partial_\phi\langle\hat{\mathcal{O}}\rangle\right|$ denotes the derivative of the measurement value with respect to ϕ. From Eq. (1), this derivative can be readily evaluated as

$$\begin{aligned}\partial_\phi\langle\hat{\mathcal{O}}\rangle &= -\mathrm{i}\langle\psi_t|I_z\hat{\mathcal{O}}|\psi_t\rangle + \mathrm{i}\langle\psi_t|\hat{\mathcal{O}}I_z|\psi_t\rangle \\ &= -\mathrm{i}\langle\psi_t|[\hat{I}_z,\hat{\mathcal{O}}]|\psi_t\rangle.\end{aligned} \tag{2}$$

Now, it is clear that we would prefer those probe states that make $\left|\langle\psi_t|[\hat{I}_z,\hat{\mathcal{O}}]|\psi_t\rangle\right|$ as large as possible and moreover, the working point of the magnetometer is chosen to be the position of minimum $\Delta\hat{\mathcal{O}}$.

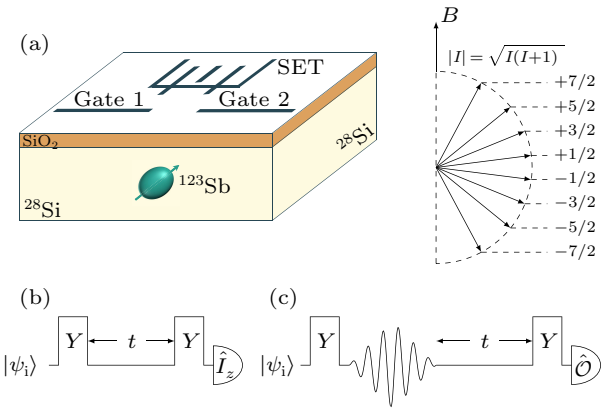


Fig. 1. (a) The false-color scanning electron micrograph of the silicon metal–oxide–semiconductor device. Eight-level structure of a single donor high-spin nucleus ^{123}Sb. (b) The schematic diagram of Ramsey measurement procedure, where Y (X) indicates the linear polarization of the microwave pulse in the laboratory frame. The accumulated phase of a superposition state during an interrogation time t allows for inference of the ambient magnetic field. (c) A general metrological experiment can be divided into three distinct parts: the preparation of a probe state, its interaction with the system to be measured and the probe readout. A spin coherent state is a specific quantum state of a spin system that most closely resembles a classical spin.

3. Beyond quantum standard limit

According to quantum metrology theory, non-classical states can achieve the goal of surpassing the SQL.[30] To generate non-classical states possessing such properties, we exploit the natural quadrupole Hamiltonian of the sample. The ^{123}Sb nucleus has non-zero electric quadrupole moment Q as it has a non-spherical charge distribution.[31] Additionally, due

to the different thermal contractions of Al and Si, the aluminum gates can cause considerable lattice strain at low temperatures, then resulting in an electric field gradient (EFG), described as $V_{ij} = \partial^2 V/\partial x_i \partial x_j$, where V is the local electrical potential of the crystal. The EFG is a real, traceless, and symmetric tensor. Working in the frame of EFG principal axes, only the diagonal components V_{xx}, V_{yy}, V_{zz} survive, the nuclear quadrupole Hamiltonian then goes[32]

$$\hat{H}_Q = \frac{f_Q}{6}\left[3\hat{I}_z^2 - \hat{I}^2 + \eta(\hat{I}_x^2 - \hat{I}_y^2)\right], \tag{3}$$

in which $f_Q = 3eQV_{zz}/(2I(2I-1))$, $\hat{I}^2 = I(I+1)$, and $\eta = (V_{xx} - V_{yy})/V_{zz}$ $(0 \le \eta \le 1)$ is the EFG biaxiality parameter indicating the asymmetry of EFG. Note that $\hat{H}_Q$ is quadratic in the nuclear spin operators, hence this nonlinear Hamiltonian could be used to generate non-classical spin states. Indeed, the two extreme cases of the quadrupole Hamiltonian $\hat{H}_Q$ in Eq. (3), namely, $\hat{H}_Q(\eta = 0) \propto \hat{H}_{\rm OAT} = \hat{I}_z^2$ and $\hat{H}_Q(\eta = 1) \propto \hat{H}_{\rm TAC} = (\hat{I}_z^2 - \hat{I}_y^2)$, correspond to the one-axis twisting (OAT) Hamiltonian and the two-axis countertwisting (TAC) Hamiltonian, respectively, which are routine for creating squeezed spin states.[33] In general cases, $\hat{H}_Q$ is a combination of OAT and TAC, and is referred to as the mixed-axis twisting (MAT) Hamiltonian.[27,34]

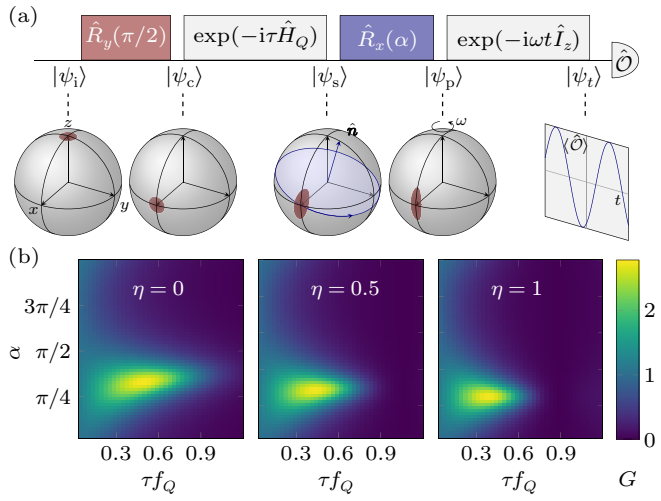


Fig. 2. (a) An illustration of the pulse sequence for generating nonclassical states via the natural quadrupole Hamiltonian, and the associated spin distributions on Bloch spheres. The system starts from $|+7/2\rangle$. After a $\pi/2$ pulse, the state $|\psi_c\rangle$ has the uncertainties $\Delta\hat{I}_x = 0$ and $\Delta\hat{I}_y = \Delta\hat{I}_z = \sqrt{I/2}$. Then $\hat{H}_Q$ twists the uncertainties so that they are redistributed, where f_Q sets the time scale of the twisting dynamics. The effect is that $\Delta\hat{I}_y$ is reduced to a certain degree depending on the twisting parameter τf_Q. (b) Simulated metrological gain for three different η values, with varying the sequence parameters τf_Q and α.

The scheme is shown in Fig. 2(a). The rotational operations are implemented with Rabi driving much faster than the quadrupole interaction so that the latter can be neglected during the rotation. The state $|\psi_p\rangle$ produced after the nonlinear dynamics by $\hat{H}_Q$ has redistributed uncertainties between certain orthogonal components in the yz plane. The consequence is that, the best magnetic sensitivity is achieved for a rotation axis $\hat{\boldsymbol{n}}_{\rm max}$ in the yz plane coinciding with the direction of the maximal spin projection variance. To detect magnetic field in the z direction, we apply a frame transformation $\hat{R}_x(\alpha)$ that turns $\hat{\boldsymbol{n}}_{\rm max}$ into $\hat{\boldsymbol{z}}$. Hence, the sequence in Fig. 2(a) results in the following state at the measurement stage:

$$|\psi_t\rangle = \mathrm{e}^{-\mathrm{i}\phi\hat{I}_z}\hat{R}_x(\alpha)\,\mathrm{e}^{-\mathrm{i}\tau\hat{H}_Q}\hat{R}_y(\pi/2)\,|+7/2\rangle\,. \tag{4}$$

Because the uncertainty $\Delta\hat{I}_y$ has been reduced, so the measurement operator is chosen to be $\hat{\mathcal{O}} = \hat{I}_y$, giving $\Delta\phi\,\big|_{|\psi_t\rangle} = \Delta\hat{I}_y/|\langle\psi_t|\hat{I}_x|\psi_t\rangle|$. To study how the application of $\hat{H}_Q$ enhances the magnetic sensitivity, we use the quantification of the increase of sensitivity by the metrological gain $G = (\Delta\phi_{\rm SQL}/\Delta\phi)^2$ and evaluate G with respect to the duration τ and the rotation angle α. The simulation results are presented in Fig. 2(b). In the case of $\eta = 0$, pure OAT leads to a maximum gain $G = 2.61$ reached for $\tau f_Q = 0.51$ and $\alpha = \pi/3$. On the other hand, when $\eta = 1$ pure TAC leads to a maximum gain $G = 2.80$ for $\tau f_Q = 0.39$ and $\alpha = \pi/4$. The data are in good agreement with the predictions in Ref. [33]. In the evaluation of G, there are three critical experimental parameters η, f_Q, and τ. The parameter η reflects the asymmetry of the electric field gradient (EFG). Once the sample is prepared, η is a fixed value ranging between 0 and 1. The parameter f_Q, approximately 66 kHz, represents the stark shift due to the electric quadrupole moment observed in current experiments.[24] According to simulations, the evolution time can be estimated to be $\tau \approx 0.5/f_Q = 7.57$ μs for $G \approx 2.8$, which is feasible in experiments since the experimental coherence time significantly exceeds τ. It can be seen from the figure that, for a fixed f_Q, the TAC reaches faster the optimal nonclassical state than the OAT. While theoretically TAC allows improved sensitivity scaling over OAT, for the present relatively small spin size, the two Hamiltonian models yield almost the same sensitivity gain.

4. Achieving the Heisenberg limit

It should be noted that the previously mentioned scheme does not yet achieve the Heisenberg limit. Here, we propose a new scheme designed to reach the Heisenberg limit, which involves the following three steps. First, we prepare a non-classical state with enhanced quantum coherence, specifically a spin cat state, to serve as our probe state. This presents a slight challenge due to the inherent strain effect η in the system's Hamiltonian as depicted in Eq. (3), which cannot be switched off. As illustrated in Fig. 3, we introduce a scheme capable of generating a cat state using a periodic multi-pulse sequence. This cat-state generation procedure is effective for any value of η. The basic sequence comprises $[\tau_c/4\text{–}\hat{R}_{-z}(\pi/2)\text{–}\tau_c/2\text{–}\hat{R}_z(\pi/2)\text{–}\tau_c/4]$, where free evolution and pulses alternate. Here, $\tau_c/2$ denotes the free time

evolution $e^{-i\hat{H}_Q\tau_c/2}$ of the Hamiltonian $\hat{H}_Q$, and $\hat{R}_z(\pi/2)$ represents the $\pi/2$ pulse around the z-axis. Thus, the evolution operator for a single period can be expressed as follows:

$$U = e^{-i\tau_c/4\hat{H}_Q}\hat{R}_z(\pi/2)\,e^{-i\tau_c/2\hat{H}_Q}\hat{R}_z^{\dagger}(\pi/2)\,e^{-i\tau_c/4\hat{H}_Q}.$$

Then, we repeat the period m times, the total evolution operator $U_{\rm tot} = U^m$. Using the relation $\hat{I}_x^2 + \hat{I}_y^2 + \hat{I}_z^2 = \hat{I}^2$ and the Baker–Campbell–Hausdorff formula,[35] we find

$$U_{\rm tot} \approx \exp\left[-i\tau_c\frac{f_Q}{6}\left(3\hat{I}_z^2 - \hat{I}^2\right)\right]. \tag{5}$$

In this way, we effectively turn off the effect η. If we require the condition $m\tau_c f_Q/2 = \pi/2$, the whole sequence for the preparation of the probe state as shown in Fig. 3 would lead to a cat state of the form[28]

$$\begin{aligned}|\psi_p\rangle &= R_x(\pi/2)U^m R_y(\pi/2)|+7/2\rangle \\ &= e^{-i5\pi/4}\left(|+7/2\rangle + |-7/2\rangle\right)/\sqrt{2}.\end{aligned} \tag{6}$$

Second, we perform the evolution $e^{-i\omega t I_z}$ to encode target parameter ω. Then we obtain the final state with ω information by $|\psi_t\rangle = e^{-i\omega t I_z}|\psi_p\rangle$. Third, we measure the final state $|\psi_t\rangle$ to extract target parameter ω. Because $|\psi_p\rangle$ is a superposition between the maximally polarized states of opposite orientation, the coherence of this state cannot be probed using the common magnetization measurement. Instead, we perform the parity measurement $\hat{\mathcal{O}} = \hat{\Pi}$ with $\hat{\Pi}$ defined by $\hat{\Pi}|m\rangle = (-1)^{I-m}|m\rangle$.[28,36] In this framework, the parity oscillation expected for the state $|\psi_p\rangle$ yields a metrological gain $G = 2I = 7$.[28] This corresponds to the Heisenberg limit for the spin I. Here, dynamical decoupling (DD) schemes can be utilized to extract the target parameter if it is an AC signal. The conventional Ramsey protocol is ineffective in this case because the accumulated phase $\phi = \omega t$ will be zero for AC signals. Instead, the DD scheme can be employed to reverse the time evolution of the qubit, allowing the phase to accumulate continuously. It also achieves longer coherence times, bounded by T_2 and not T_2^* as in the Ramsey sequence.

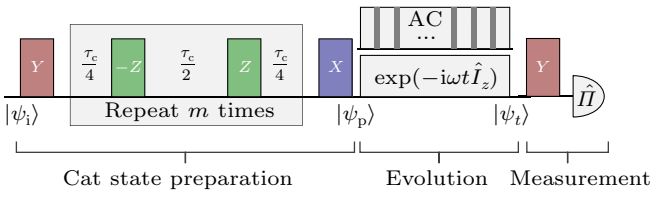


Fig. 3. An illustration of the proposed scheme to achieve the Heisenberg limit is outlined, consisting of three steps. Initially, a periodic multi-pulse sequence is used to prepare the spin cat state. This is followed by dynamical evolution that encodes the target parameter ω. Finally, a parity measurement is conducted. In this scheme, X, Y, and Z represent $\pi/2$ pulses around the x, y, and z axes, respectively, and τ_c denotes the free time evolution under the Hamiltonian $\hat{H}_Q$. For AC signals, the DD schemes can be used to accumulate the phase continuously. The black bars represent the π DD pulses used for detecting AC signals.

5. The sensitivity analysis

The sensitivity of the magnetometer is affected by various practical noises, including spin projection noise, ambient magnetic field noise, and quantum noise. Spin projection noise represents the most fundamental source of estimation uncertainty, as it depends on the number of spin projection measurements. The presence of ambient magnetic field noise around qubits leads to decoherence during the sensing period, thereby reducing the sensitivity by a factor of $e^{\chi(t)}$. Here, $\chi(t)$ represents the decoherence function, which characterizes the noise processes from the ambient magnetic field noise, such as $\chi(t) = t/T_2^*$ for unentangled states and $\chi(t) = 4I^2 t/T_2^*$ for spin-I cat states. In addition to the previously mentioned noises, other quantum noises such as state initialization and qubit manipulation errors also impact the sensitivity. These errors similarly result in a reduction of sensitivity by a factor β. Unlike the decoherence effect, this reduction is independent of the sensing time because β is a constant. The factor $\beta < 1$ can be defined as the fidelity of the final state, taking into account the infidelity of spin initialization and control imperfections.[37] After considering these noises, the sensitivity ΔB can be defined as[38]

$$\Delta B^{\rm single} = \frac{e^{\chi(t)}}{\beta\gamma\sqrt{t}}\frac{\Delta\hat{\mathcal{O}}}{|\partial\langle\hat{\mathcal{O}}\rangle/\partial\phi|},\quad \Delta B^{\rm ensemble} = \frac{\Delta B^{\rm single}}{\sqrt{n}}. \tag{7}$$

Here, γ and T_2^* represent the gyromagnetic ratio and dephasing time of the spin, respectively. n indicates the spin density per unit volume. $|\partial\langle\hat{\mathcal{O}}\rangle/\partial\phi|$ is the derivative of the measurement outcome with respect to $\phi = \gamma B t$. Employing non-classical states and high-spin nuclei can reduce the phase uncertainty, $\Delta\phi = \frac{\Delta\hat{\mathcal{O}}}{|\partial\langle\hat{\mathcal{O}}\rangle/\partial\phi|}$. For example, in our proposed scheme, $\Delta\phi$ can achieve a minimum value of $1/(2I)$, reaching the Heisenberg limit. While increasing the phase accumulation time t enhances sensitivity, it must be noted that the free precession signal may decay due to environmental perturbations. This constitutes the main finding of our paper.

Magnetometers based on high spin nuclei, such as the ^{123}Sb nucleus, exhibit distinct features compared with NV center magnetometers, in terms of sensitivity and applications. The sensitivity, denoted as ΔB, primarily depends on several key factors: the gyromagnetic ratio γ, the dephasing time T_2^*, the spin density n, and the spin quantum number I. The magnetic sensitivities for high spin nuclei and NV centers can be respectively written as $\Delta B_{\rm n} = \frac{e^{4I^2 t/T_2^*}}{2I\beta\gamma\sqrt{nt}}$ and $\Delta B_{\rm e} = \frac{e^{t/T_2^*}}{\beta\gamma\sqrt{nt}}$. For instance, the ^{123}Sb nucleus has a spin quantum number $I = 7/2$, compared to $I = 1$ for NV electrons, yielding an enhanced sensitivity. Additionally, the nuclear gyromagnetic ratio of ^{123}Sb is $\gamma_{\rm n} = -5.553$ MHz/T, lower than the electron gyromagnetic ratio of $\gamma_{\rm e} = 27.97$ GHz/T,

which results in a decrease by about 5000 times. Regarding the coherence time, the nuclear spin in silicon has a dephasing time $T_2^* = 600$ ms,[39] significantly longer than the 36 μs observed for electron spins,[40] thus improving by a factor of approximately 130. Moreover, experimental data suggest that β values for ^{123}Sb can exceed 90%,[41] whereas for NV centers, $\beta \sim 1$.[37] For spin density, NV centers maintain a safe density of 10^{16} cm^{-3} without destroying coherence time,[15] while nuclear spins can reach up to 10^{22} cm^{-3} due to the significantly smaller gyromagnetic ratio.[42] An estimated sensitivity of $\Delta B^{\text{ensemble}}$ for ^{123}Sb-based magnetometers may reach 6 aT·Hz$^{-1/2}$·cm$^{-3/2}$, better than the roughly estimated 139 aT·Hz$^{-1/2}$·cm$^{-3/2}$ for NV centers. Additionally, similar to NV centers, ^{123}Sb can be engineered into a single-spin sensor with sub-10 nm spatial resolution when placed near the bulk silicon surface within a probe setup, ideal for nanoscale magnetic detection and imaging. Unlike NV centers that require lasers for initialization and readout, which can damage light-sensitive samples, this sensor utilizes local electronic fields for these processes, making them preferable for applications involving photosensitive samples.

6. Conclusion and outlook

In conclusion, we have demonstrated a novel highly nuclear spin magnetometer with quantum-enhanced effect. This constitutes a solid-state magnetic sensor, holding the promise of miniaturization. We use quadrupolar coupling to drive the nuclear spin $I = 7/2$ of ^{123}Sb doped in silicon under a non-linear one-axis twisting Hamiltonian. We exploit the quadrupolar nuclei to generate spin-squeezed state, performing as the initial state of Ramsey experiment. Decreased quantum fluctuation yields higher sensitivity beyond the shot-noise limit. In future, to further push the sensitivity limit, we can exploit advanced dynamical decoupling techniques (e.g., spin echo, CPMG[43] or MREV[44,45] pulse sequences) to make the spin experience an isotropic Hamiltonian commuted with signal perturbation, then inducing desired evolution. Since NER has much in common with NV center, it is thence reasonable that quantum optimal control[46] and robust control[47] that already proved useful in NV sensing should also be applicable here. Related theoretical works include variational optimization algorithms.[48–51] Alkali-metal atomic magnetometers, based on detection of Larmor spin precession of optically pumped atoms in a magnetic field, have comparable sensitivity with large measurement volumes, then have much lower sensitivity and resolution in magnetic imaging applications with more compact designs.[52] Recently there has also been theoretical work[53] that reveals some fundamental limit in respect of the trade-off between sensitivity and resolution. Our sensor will find applications in fundamental physics tests, quantum computing, medical and biological imaging, surface physics and material science. Future work will also investigate the potential of NER magnetometer working in challenging environments.[54] As a solid-state platform for compact quantum sensors, NER is promising to perform.

Acknowledgments

Project supported by the National Natural Science Foundation of China (Grant Nos. 1212200199, 12122506, 12004165, 12275117, and 12204230), Guangdong Basic and Applied Basic Research Foundation (Grant Nos. 2021B1515020070 and 2022B1515020074), Guangdong Provincial Key Laboratory (Grant No. 2019B121203002), and Shen-zhen Science and Technology Program (Grant Nos. KQTD20200820113010023, RCBS20200714114820298, and RCYX20200714114522109).

References

[1] Degen C L, Reinhard F and Cappellaro P 2017 *Rev. Mod. Phys.* **89** 035002
[2] Budker D and Kimball D F J 2013 *Optical Magnetometry* (Cambridge University Press)
[3] Safronova M S, Budker D, DeMille D, Kimball D F J, Derevianko A and Clark C W 2018 *Rev. Mod. Phys.* **90** 025008
[4] Casola F, van der Sar T and Yacoby A 2018 *Nat. Rev. Mater.* **3** 17088
[5] Boto E, Meyer S S, Shah V, Alem O, Knappe S, Kruger P, Fromhold T M, Lim M, Glover P M, Morris P G, Bowtell R, Barnes G R and Brookes M J 2017 *Neuroimage* **149** 404
[6] Harel E, Schröder L and Xu S 2008 *Annu. Rev. Anal. Chem.* **1** 133
[7] Czap G, Wagner P J, Xue F, Gu L, Li J, Yao J, Wu R and Ho W 2019 *Science* **364** 670
[8] Clarke J and Braginski A I 2004 *The SQUID Handbook* (Wiley-VCH, Weinheim)
[9] Budker D and Romalis M 2007 *Nat. Phys.* **3** 227
[10] Wasilewski W, Jensen K, Krauter H, Renema J J, Balabas M V and Polzik E S 2010 *Phys. Rev. Lett.* **104** 133601
[11] Muessel W, Strobel H, Linnemann D, Hume D B and Oberthaler M K 2014 *Phys. Rev. Lett.* **113** 103004
[12] Ruster T, Kaufmann H, Luda M A, Kaushal V, Schmiegelow C T, Schmidt-Kaler F and Poschinger U G 2017 *Phys. Rev. X* **7** 031050
[13] Bassett L C, Alkauskas A, Exarhos A L and Fu K M C 2019 *Nanophotonics* **8** 1867
[14] Balasubramanian G, Chan I Y, Kolesov R, Al-Hmoud M, Tisler J, Shin C, Kim C, Wojcik A, Hemmer P R, Krueger A, Hanke T, Leitenstorfer A, Bratschitsch R, Jelezko F and Wrachtrup J 2008 *Nature* **455** 648
[15] Taylor J M, Cappellaro P, Childress L, Jiang L, Budker D, Hemmer P R, Yacoby A, Walsworth R and Lukin M D 2008 *Nat. Phys.* **4** 810
[16] Schirhagl R, Chang K, Loretz M and Degen C L 2014 *Annu. Rev. Anal. Chem.* **65** 83
[17] Liu Y X, Ajoy A and Cappellaro P 2019 *Phys. Rev. Lett.* **122** 100501
[18] Chen M, Meng C, Zhang Q, Duan C, Shi F and Du J 2018 *Natl. Sci. Rev.* **5** 346
[19] Barry J F, Schloss J M, Bauch E, Turner M J, Hart C A, Pham L M and Walsworth R L 2020 *Rev. Mod. Phys.* **92** 015004
[20] Baumgart I, Cai J M, Retzker A, Plenio M B and Wunderlich C 2016 *Phys. Rev. Lett.* **116** 240801
[21] Dietsche E K, Larrouy A, Haroche S, Raimond J M, Brune M and Gleyzes S 2019 *Nat. Phys.* **15** 326
[22] Mamin H J, Sherwood M H, Kim M, Rettner C T, Ohno K, Awschalom D D and Rugar D 2014 *Phys. Rev. Lett.* **113** 030803
[23] Cooper A, Sun W K C, Jaskula J C and Cappellaro P 2019 *Phys. Rev. Appl.* **12** 044047
[24] Asaad S, Mourik V, Joecker B, Johnson M A I, Baczewski A D, Firgau H R, Madzik M T, Schmitt V, Pla J J, Hudson F E, Itoh K M, McCallum J C, Dzurak A S, Laucht A and Morello A 2020 *Nature* **579** 205
[25] Morello A, Pla J J, Bertet P and Jamieson D N 2020 *Adv. Quantum Technol.* **3** 2000005

[26] Auccaise R, Araujo-Ferreira A G, Sarthour R S, Oliveira I S, Bonagamba T J and Roditi I 2015 *Phys. Rev. Lett.* **114** 043604
[27] Korkmaz Y A and Bulutay C 2016 *Phys. Rev. A* **93** 013812
[28] Birrittella R J, Alsing P M and Gerry C C 2021 *Phys. Rev. A* **3** 014701
[29] Giovannetti V, Lloyd S and Maccone L 2011 *Nat. Photon.* **5** 222
[30] Pezzè L, Smerzi A, Oberthaler M K, Schmied R and Treutlein P 2018 *Rev. Mod. Phys.* **90** 035005
[31] Haiduke R L A and da Silva A B F 2006 *J. Chem. Phys.* **125** 064301
[32] Abragam A 1961 *The Principles of Nuclear Magnetism* (Oxford University Press)
[33] Kitagawa M and Ueda M 1993 *Phys. Rev. A* **47** 5138
[34] Bian Z W and Lai X B 2013 *Int. J. Theor. Phys.* **52** 3922
[35] Gilmore R 1974 *J. Math. Phys.* **15** 2090
[36] Bollinger J J, Itano W M, Wineland D J and Heinzen D J 1996 *Phys. Rev. A* **54** R4649
[37] Xie T, Zhao Z, Kong X, Ma W, Wang M, Ye X, Yu P, Yang Z, Xu S, Wang P, *et al.* 2021 *Sci. Adv.* **7** eabg9204
[38] Barry J F, Schloss J M, Bauch E, Turner M J, Hart C A, Pham L M and Walsworth R L 2020 *Rev. Mod. Phys.* **92** 015004
[39] Muhonen J T, Dehollain J P, Laucht A, Hudson F E, Kalra R, Sekiguchi T, Itoh K M, Jamieson D N, McCallum J C, Dzurak A S, *et al.* 2014 *Nat. Nanotechnol.* **9** 986
[40] Liu W, Wu Y, Duan C K, Rong X and Du J 2021 *Phys. Rev. Lett.* **126** 170506
[41] Yu X, Wilhelm B, Holmes D, Vaartjes A, Schwienbacher D, Nurizzo M, Kringhøj A, van Blankenstein M R, Jakob A M, Gupta P, *et al.* 2024 arXiv:2405.15494 [quant-ph]
[42] McCallum J, Johnson B and Botzem T 2021 *Appl. Phys. Rev.* **8** 031314
[43] Meiboom S and Gill D 1958 *Rev. Sci. Instrum.* **29** 688
[44] Khodjasteh K and Lidar D A 2007 *Phys. Rev. A* **75** 062310
[45] Mansfield P 1971 *J. Phys. C: Solid State Phys.* **4** 1444
[46] Nöbauer T, Angerer A, Bartels B, Trupke M, Rotter S, Schmiedmayer J, Mintert F and Majer J 2015 *Phys. Rev. Lett.* **115** 190801
[47] Wang Z Y, Lang J E, Schmitt S, Lang J, Casanova J, McGuinness L, Monteiro T S, Jelezko F and Plenio M B 2019 *Phys. Rev. Lett.* **122** 200403
[48] Li J, Yang X, Peng X and Sun C P 2017 *Phys. Rev. Lett.* **118** 150503
[49] Koczor B, Endo S, Jones T, Matsuzaki Y and Benjamin S C 2020 *New J. Phys.* **22** 083038
[50] Yang X, Thompson J, Wu Z, Gu M, Peng X and Du J 2020 *npj Quantum Inf.* **6** 62
[51] Meyer J J, Borregaard J and Eisert J 2021 *npj Quantum Inf.* **7** 89
[52] Affolderbach C, Stähler M, Knappe S and Wynands R 2002 *Appl. Phys. B* **75** 605
[53] Mitchell M W and Palacios Alvarez S 2020 *Rev. Mod. Phys.* **92** 021001
[54] Fu K M C, Iwata G Z, Wickenbrock A and Budker D 2020 *AVS Quantum Sci.* **2** 044702